



ORIGINAL PAPER

Farouk Yahia Addou · Abdelhakim Kaci ·
Abdeldjebbar Tounsi · Abdelmoumen Anis Bousahla ·
Abdelouahed Tounsi · Mohammed A. Al-Osta ·
Sherain M. Y. Mohamed · Saad Althobaiti ·
Mahmoud M. Selim

Static behavior of FG sandwich beams under various boundary conditions using trigonometric series solutions and refined hyperbolic theory

Received: 18 June 2024 / Revised: 4 July 2024 / Accepted: 13 July 2024

© The Author(s), under exclusive licence to Springer-Verlag GmbH Austria, part of Springer Nature 2024

Abstract A refined hyperbolic shear deformation theory is presented to analyze the mechanical behavior of isotropic and sandwich functionally graded material (FGM) beams under various boundary conditions. The material properties are considered to be isotropic at each point and change across the thickness direction. The volume fraction gradation follows a power law distribution with respect to the FGM core or skins of the beam. The solution is attained by minimizing the total potential energy. This recent theory is a new type of third-order shear deformation theory that includes undetermined integral variables. The recent theory describes the variation of transverse shear strains throughout the thickness of a beam. It shows how these strains satisfy the zero traction boundary conditions on the top and bottom surfaces, all without the need for shear correction factors. An analytical solution based on trigonometric series is developed to solve the problem while satisfying various boundary conditions. Comparative studies are conducted to validate the accuracy and efficiency of this method. The current model can accurately predict the static responses of functionally graded isotropic and sandwich beams with arbitrary boundary conditions.

F. Y. Addou
Civil Engineering Department, Faculty of Science and Technology, University of Mostaganem, Mostaganem, Algeria

F. Y. Addou · A. Kaci · A. Tounsi · A. Tounsi (✉)
Material and Hydrology Laboratory, Civil Engineering Department, Faculty of Technology,
University of Sidi Bel Abbès, Sidi Bel Abbès, Algeria
e-mail: tou_abdel@yahoo.com

A. Kaci
Département de Génie Civil et Hydraulique, Faculté de Technologie, Université Dr. Tahar Moulay, Cité En-Nasr,
BP 138, 20000 Saida, Algeria

A. Tounsi
Mechanical Engineering Department, Faculty of Science and Technology, University of Relizane, Relizane, Algeria

A. A. Bousahla
Laboratoire de Modélisation et Simulation Multi-échelle, Université de Sidi Bel Abbès, Sidi Bel Abbès, Algeria

A. Tounsi · M. A. Al-Osta
Department of Civil and Environmental Engineering, King Fahd University of Petroleum and Minerals, 31261 Dhahran, Eastern
Province, Saudi Arabia

A. Tounsi · M. A. Al-Osta
Interdisciplinary Research Center for Construction and Building Materials, KFUPM, 31261 Dhahran, Saudi Arabia

S. M. Y. Mohamed · M. M. Selim
Department of Mathematics, College of Science and Humanities, Prince Sattam Bin Abdulaziz University, 11942 Al-Kharj,
Saudi Arabia

S. Althobaiti
Department of Sciences and Technology, Ranyah University Collage, Taif University, P.O. Box 11099, 21944 Taif, Saudi Arabia

1 Introduction

The need for enhanced structural efficiency in various engineering disciplines has prompted the creation of a novel category of materials called functionally graded materials (FGMs) [1–3]. FGMs are composites whose material properties change gradually over one or more directions. This is accomplished by adjusting the volume fraction along the thickness direction and blending two different materials [4]. This continuously changing composition eliminates interface issues, resulting in smooth stress distributions. FGMs are now widely used as structural elements in various applications. The FGM concept has applications in several engineering fields such as aerospace, civil engineering, nuclear, automotive, energy, and biomaterials [4–16].

In recent years, much research has been conducted to predict the structural responses of FG beams accurately. The three basic categories for categorizing beam problems are beam theory and solution strategies. The three types of solution techniques are analytical solutions, elasticity solutions, and numerical solutions. The availability of exact elasticity solutions is crucial for researchers since they are used as a standard for comparing solutions derived from approximate beam theories. However, due to the amount of difficulty and the computer component required, relatively few researchers have made contributions to obtaining precise elasticity answers for the investigation of the behavior of FG beams [17–26]. Exact elasticity solutions are actually computationally time-consuming, analytically challenging, and impractical for real-world issues. Hence, approximate one- and two-dimensional theories are derived by applying specific kinematic assumptions. The beam theory consists of classical beam theory (CBT), first-order beam theory (FBT), and higher-order theory (HBT). It is important to note that CBT is only appropriate for thin beams because it neglects the shear effect [27–32]. FBT yields acceptable results but relies on the shear correction factor, which is difficult to establish because of its dependence on many parameters. Consequently, this theory has been increasingly utilized to predict responses of FG beams [33–38]. Higher-order shear deformation theories (HSDTs) have been developed to account for shear deformation effects. These theories are based on a nonlinear variation across the thickness of the in-plane displacements. The HSDTs ensure that there are zero shear stress conditions at the top and bottom surfaces of the beams, eliminating the need for a shear correction factor [39–50]. Although analytical methods lead to accurate solutions, their uses are limited to problems with simpler geometries, limits, and loading conditions. As a result, numerical methods are needed to solve more complex problems. Numerical methods used by researchers to study the behavior of FG structures are the Ritz method, state-space method, Galerkin method, differential quadrature method, Lagrange multiplier method, and Chebyshev collocation method [44, 51–76]. Recent studies have continued to employ and develop these methods. Abbaslou et al. [77] explored the vibration and dynamic instability of functionally graded porous doubly curved panels with piezoelectric layers in supersonic airflow, using the Galerkin method to discretize the equations of motion. Ebrahimi and Parsi [78] investigated wave propagation in functionally graded graphene origami-enabled auxetic metamaterial beams on an elastic foundation, determining the analytical solution of the governing equations. Yaylacı et al. [79] conducted a numerical study on the vibration and buckling of FG beams with edge cracks using the finite element method (FEM) and multilayer perceptron (MLP). Hai et al. [80] used a refined plate theory and the Galerkin method to investigate the influence of micromechanical models on the behavior of FG plates under different boundary conditions. Zhang et al. [81] focused on the buckling behavior of two-dimensional functionally graded (2D-FG) nanosize tubes, including porosity, based on the first shear deformation and higher-order theory, solving the derived equations numerically for various boundary conditions. Cho [82] analyzed the static and free vibration of functionally graded porous plates using neutral surface theory and the natural element method (NEM). Ghatage and Sudhagar [83] examined the free vibrational responses of bidirectional axially graded cylindrical shell panels using 3D graded finite element approximation under a temperature field. Tayebi et al. [84] applied the full layerwise finite element method (FEM) in the free vibration analysis of FG composite plates reinforced with graphene nanoplatelets (GPLs) in a thermal environment. Gholami et al. [85] investigated the free vibration behavior of bi-dimensional functionally graded (BFG) nanobeams under various boundary conditions using the variable substitution method to formulate the state-space differential equations and the dynamic stiffness matrix. Wu [86] examined the nonlinear finite element vibration analysis of functionally graded nanocomposite spherical shells reinforced with graphene platelets. Xu and She [87] studied the thermal post-buckling and primary resonance of porous functionally graded material (FGM) beams in a thermal environment using the two-step perturbation method. Finally, Fan et al. [88] investigated the thermal buckling of a nonuniform nanobeam made of functionally graded material using classical beam theories and Eringen's nonlocal elasticity, solving the nonlocal partial differential equations with the generalized differential quadrature method (GDQM).

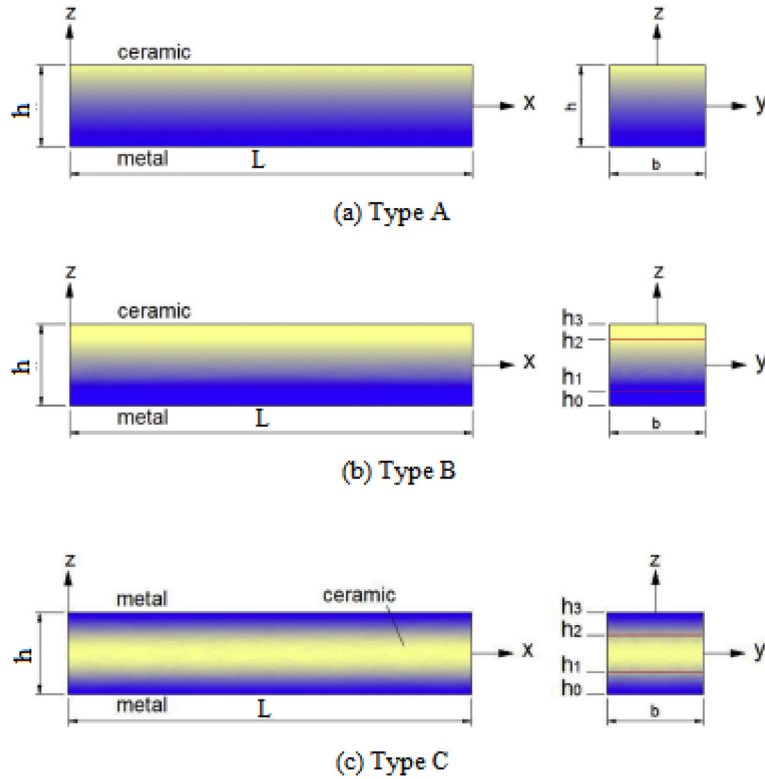


Fig. 1 Isotropic and FGSB geometry

Sandwich structures have received significant attention in various engineering applications. There has been a proposal for sandwich structures made of materials with gradients of properties (FG). The core or two skins have materials with gradient properties (FGM) due to the remarkable advantages of FGM. Many research papers have been developed to analyze sandwich structures [89–98].

This paper investigates the influences of boundary conditions on the static behavior of isotropic and sandwich FG beams using the Ritz method enhanced with a novel trigonometric series and a recently refined shear deformation theory. The proposed theories have been designed to fulfill the zero traction boundary conditions on both the top and bottom surfaces of the beam, thereby eliminating the need for a shear correction factor. The accuracy of the proposed solution was validated through rigorous convergence and verification studies. Numerical results are presented for various boundary conditions to analyze the impact of length-to-depth ratio, boundary conditions, power law index skin–core–skin thickness ratios, and configurations on the structural response of isotropic and sandwich functionally graded beams (SFGB). This study contributes to advancing our understanding of FGM applications in enhancing structural efficiency across multiple engineering domains.

2 Theoretical formulation

An FG beam made of ceramic–metal is being investigated. It has a length of L and a rectangular cross section with dimensions $b \times h$, as shown in Fig. 1. This study examines three types of FG beams: (1) Type A, which refers to isotropic FG beams, (2) Type B, which denotes sandwich beams (SB) with FG core and homogeneous faces, and (3) Type C, which represents SB with FG faces and homogeneous core. The rectangular Cartesian coordinate system describes small deformations of three layers of the sandwich elastic beam within the unstressed reference configuration. The midplane is defined by $z = 0$, and its external bounding planes are defined by $z = \pm h/2$. Three elastic layers are defined by “Layer 1”, “Layer 2”, and “Layer 3” from the bottom layer to the top layer. The vertical positions of the base, the two interfaces, and the top are represented by $h_0 = -h/2$, h_1 , h_2 , and $h_3 = h/2$, respectively. In the current study, the SB is subjected to compressive in-plane forces acting on the midplane of the beam.

2.1 Type A

The beam of type A has a graded structure, transitioning from ceramic at the top surface to metal at the bottom surface (see Fig. 1a). The ceramic phase's volume fraction is determined using a simple rule of mixtures as follows:

$$V_c(z) = \left(\frac{2z + h}{2h} \right)^p \quad (1)$$

where V_c represents the volume fraction function of ceramic, and p denotes the volume fraction index ($0 \leq p \leq +\infty$) that determines the material change profile across h .

2.2 Type B

The core layer of the material transitions from a metal composition at the bottom to a ceramic composition at the top. The upper face is composed of isotropic ceramic, while the lower face is made of isotropic metal (refer to Fig. 1b). The volume fraction of the ceramic phase is determined using a straightforward rule of mixtures as follows:

$$\begin{aligned} V_c^{(1)} &= 0 & z \in [h_0, h_1] \\ V_c^{(2)} &= \left(\frac{z-h_1}{h_2-h_1} \right)^p & z \in [h_1, h_2] \\ V_c^{(3)} &= 1 & z \in [h_2, h_3] \end{aligned} \quad (2)$$

where $V^{(n)}$ ($n = 1, 2, 3$) indicates the volume fraction function of layer n ; p is the volume fraction index ($0 \leq p \leq +\infty$) that determines the material change profile across h .

2.3 Type C

The faces range from ceramic to metal, with an isotropic ceramic core (Fig. 1c). The volume fraction of the ceramic phase is calculated using a simple rule of mixtures as follows:

$$\begin{aligned} V_c^{(1)} &= \left(\frac{z-h_0}{h_1-h_0} \right)^p & z \in [h_0, h_1] \\ V_c^{(2)} &= 1 & z \in [h_1, h_2] \\ V_c^{(3)} &= \left(\frac{z-h_3}{h_2-h_3} \right)^p & z \in [h_2, h_3] \end{aligned} \quad (3)$$

where $V^{(n)}$ ($n = 1, 2, 3$) indicates the layer n 's volume fraction function; p is the volume fraction index ($0 \leq p \leq +\infty$) that determines the material change profile across h .

The effective material properties for the n th layers, like Young's modulus $E^{(n)}$ and Poisson's ratio, $\nu^{(n)}$, are determined by the linear rule of the mixture as

$$P^{(n)}(z) = P_m + (P_c - P_m)V^{(n)} \quad (4)$$

where subscripts m and c represent metal and ceramic, respectively.

The study assumes that the Poisson's ratio of the plate remains constant throughout, as its influence on deformation is considerably less significant than that of Young's modulus.

2.4 Kinematics and constitutive equations

The displacement field that fulfills the requirements for transverse shear stresses to be zero at a specific point on the top and bottom surfaces of the plate is as follows [99, 100]:

$$\begin{aligned} u(x, z) &= u_0(x) - z \frac{\partial w_0}{\partial x} + k_1 f(z) \int \theta(x) dx \\ w(x, z) &= w_0(x) \end{aligned} \quad (5)$$

Table 1 Value of A' and k_1 for different boundary conditions

Boundary conditions	A'	k_1
S-S	$-\frac{1}{\alpha^2}$	α^2
C-F	$-\frac{4}{\alpha^2}$	$\frac{\alpha^2}{4}$
C-C	$-\frac{1}{4\alpha^2}$	$4\alpha^2$

The coefficient k_1 depends on the geometry, and the $f(z)$ represents the hyperbolic shape function selected in the form [101]

$$f(z) = z(\cosh(z/h) - 1.388) \quad (6)$$

where (u, w) are the displacement components of a general point (x, z) in the FG beam, (u_0, w_0, θ) are three unknown displacements of the midplane of the beam, and h is the beam thickness. Using the displacement field in Eq. (5), the linear strains ε_{ij} are obtained as:

$$\varepsilon_x = \varepsilon_x^0 + zk_x^b + f(z)k_x^s \quad (7a)$$

$$\gamma_{xz} = g(z)\gamma_{xz}^0, \quad (7b)$$

where

$$\varepsilon_x^0 = \frac{\partial u_0}{\partial x}, \quad k_x^b = -\frac{\partial^2 w_0}{\partial x^2}, \quad k_x^s = k_1\theta, \quad (8a)$$

$$\gamma_{xz}^0 = k_1 \int \theta \, dx \quad (8b)$$

The integrals defined in the equations above will be solved using a specific method and are found as follows:

$$\int \theta \, dx = A' \frac{\partial \theta}{\partial x} \quad (9)$$

The coefficient A' is expressed based on the type of solution used, such as a trigonometric series for different boundary conditions.

Therefore, A' and k_1 are expressed in Table 1, noting that $\alpha = m\pi/L$ as follows.

The constitutive relations of an FG beam are expressed as

$$\sigma_{xx} = E(z) \varepsilon_x \quad (10a)$$

$$\tau_{xz} = G\gamma_{xz} \quad (10b)$$

where

$$G(z) = \frac{E(z)}{2(1+\nu)} \quad (10c)$$

where (σ_{xx}, τ_{yz}) and $(\varepsilon_x, \gamma_{yz})$ are the stress and strain components, respectively.

2.5 Variational formulation

The beam's strain energy from the normal force, shear force, moment, and higher-order terms is given as follows:

$$U = \frac{1}{2} \int_V \left(N_x \varepsilon_x^0 + M_x k_x^b + S_x k_x^s + Q_{xz} \gamma_{xz}^0 \right) dx, \quad (11)$$

where

$$(N_x, M_x, S_x) = \int_{-h/2}^{h/2} (1, z, f) \sigma_{xx} dz, \quad (12a)$$

$$Q_{xz} = \int_{-h/2}^{h/2} g(z) \tau_{xz} dz, \quad (12b)$$

Replacing Eq. (12) into Eq. (11), one can calculate the strain energy using the following formula:

$$U = \frac{1}{2} \int_0^L \left[A(\varepsilon_x^0)^2 + 2B\varepsilon_x^0 k_x^b + 2B^s \varepsilon_x^0 k_x^s + D(k_x^b)^2 + 2D^s k_x^b k_x^s + H^s (k_x^s)^2 + A^s (\gamma_{xz}^0)^2 \right] dx \quad (13)$$

where $(A, B, D, B^s, D^s, H^s, A^s)$ are the stiffness components of beams and can be determined by

$$(A, B, D, B^s, D^s, H^s) = \int_{-h/2}^{h/2} (1, z, z^2, f(z), zf(z), [f(z)]^2) E dz; \quad A^s = \int_{-h/2}^{h/2} [g(z)]^2 G dz \quad (14)$$

To define the strain energy equation, Eq. (8) is substituted into Eq. (13). Therefore, the strain energy equation was obtained in the form of displacement and rotation functions as follows:

$$U = \frac{1}{2} \int_0^L \left[A(u_{0,x})^2 - 2B u_{0,x} w_{0,xx} + 2k_1 B^s u_{0,x} \theta + D(w_{0,xx})^2 - 2k_1 D^s w_{0,xx} \theta + k_1^2 H^s \theta^2 + k_1^2 A^2 A^s (\theta_{,x})^2 \right] dx \quad (15)$$

The work done V by transverse load q is obtained by:

$$V = - \int_0^L q w_0 dx \quad (16)$$

The FG beams total potential energy can be determined by:

$$\begin{aligned} \Pi &= U + V \\ \Pi &= \frac{1}{2} \int_0^L \left[A(u_{0,x})^2 - 2B u_{0,x} w_{0,xx} + 2k_1 B^s u_{0,x} \theta + D(w_{0,xx})^2 - 2k_1 D^s w_{0,xx} \theta + k_1^2 H^s \theta^2 + k_1^2 A^2 A^s (\theta_{,x})^2 \right] dx - \int_0^L q w_0 dx \end{aligned} \quad (17)$$

The displacement field in Eq. (17) can be estimated using the Ritz method [102] in the following forms:

$$u_0(x) = \sum_{j=1}^m a_j \psi_j(x)$$

Table 2 Shape functions trigonometric series

Boundary conditions	$\psi_j(x)$	$\phi_j(x)$	$\xi_j(x)$
S-S	$\cos \frac{j\pi}{L}x$	$\sin \frac{j\pi}{L}x$	$\sin \frac{j\pi}{L}x$
C-F	$\sin \frac{(2j-1)\pi}{2L}x$	$1 - \cos \frac{(2j-1)\pi}{2L}x$	$\cos \frac{(2j-1)\pi}{2L}x$
C-C	$\sin \frac{2j\pi}{L}x$	$\sin^2 \frac{j\pi}{L}x$	$\cos \frac{2j\pi}{L}x$

Table 3 Different boundary conditions of beams

Boundary conditions	S-S	C-F	C-C
$x = 0$	$w_0 = 0$	$u_0 = 0, w_0 = 0, \theta_{,x} = 0, w_{0,x} = 0$	$u_0 = 0, w_0 = 0, \theta_{,x} = 0, w_{0,x} = 0$
$x = L$		–	

$$w_0(x) = \sum_{j=1}^m c_j \phi_j(x)$$

$$\theta(x) = \sum_{j=1}^m d_j \xi_j(x) \quad (18)$$

where (a_j, c_j, d_j) are unknown values to be obtained; $\xi_j(x)$, $\phi_j(x)$ and $\psi_j(x)$ are the shape functions that are suggested for different boundary conditions simply supported (S-S), clamped-clamped (C-C), and clamped-free (C-F) as illustrated in Table 2.

The suggested shape functions satisfy the boundary constraints in Table 3. It has been noticed that improper shape functions might result in numerical instability and sluggish convergence rates [103, 104]. Moreover, the Lagrangian multipliers technique can establish boundary constraints for shape functions that do not meet them [105–107].

By putting Eq. (18) into Eq. (17) and applying Lagrange's equations, the governing equations of motion are found by:

$$\frac{\partial \Pi}{\partial q_j} = 0 \quad (19)$$

with q_j indicating the values of (a_j, c_j, d_j) , which leads to:

$$\begin{bmatrix} K^{11} & K^{12} & K^{13} \\ {}^T K^{12} & K^{22} & K^{23} \\ {}^T K^{13} & {}^T K^{23} & K^{33} \end{bmatrix} \begin{Bmatrix} a \\ c \\ d \end{Bmatrix} = \begin{Bmatrix} 0 \\ F \\ 0 \end{Bmatrix} \quad (20)$$

where K denotes the stiffness matrix, and M represents the mass matrix and can be determined by:

$$K_{ij}^{11} = A \int_0^L \psi_{i,x} \psi_{j,x} dx, \quad K_{ij}^{12} = -B \int_0^L \psi_{i,x} \phi_{j,xx} dx, \quad K_{ij}^{13} = -B^s k_1 \int_0^L \psi_{i,x} \xi_j dx,$$

$$K_{ij}^{22} = D \int_0^L \phi_{i,xx} \phi_{j,xx} dx - N_0 \int_0^L \phi_{i,x} \phi_{j,x} dx, \quad K_{ij}^{23} = -k_1 D^s \int_0^L \phi_{i,xx} \xi_j dx,$$

$$K_{ij}^{33} = k_1^2 H^s \int_0^L \xi_i \xi_j dx + (k_1 A')^2 A^s \int_0^L \xi_{i,x} \xi_{j,x} dx, \quad F_i = \int_0^L q \phi_i dx \quad (21)$$

By resolving Eq. (20), it is possible to estimate the deflection and stresses of isotropic and FG sandwich beams.

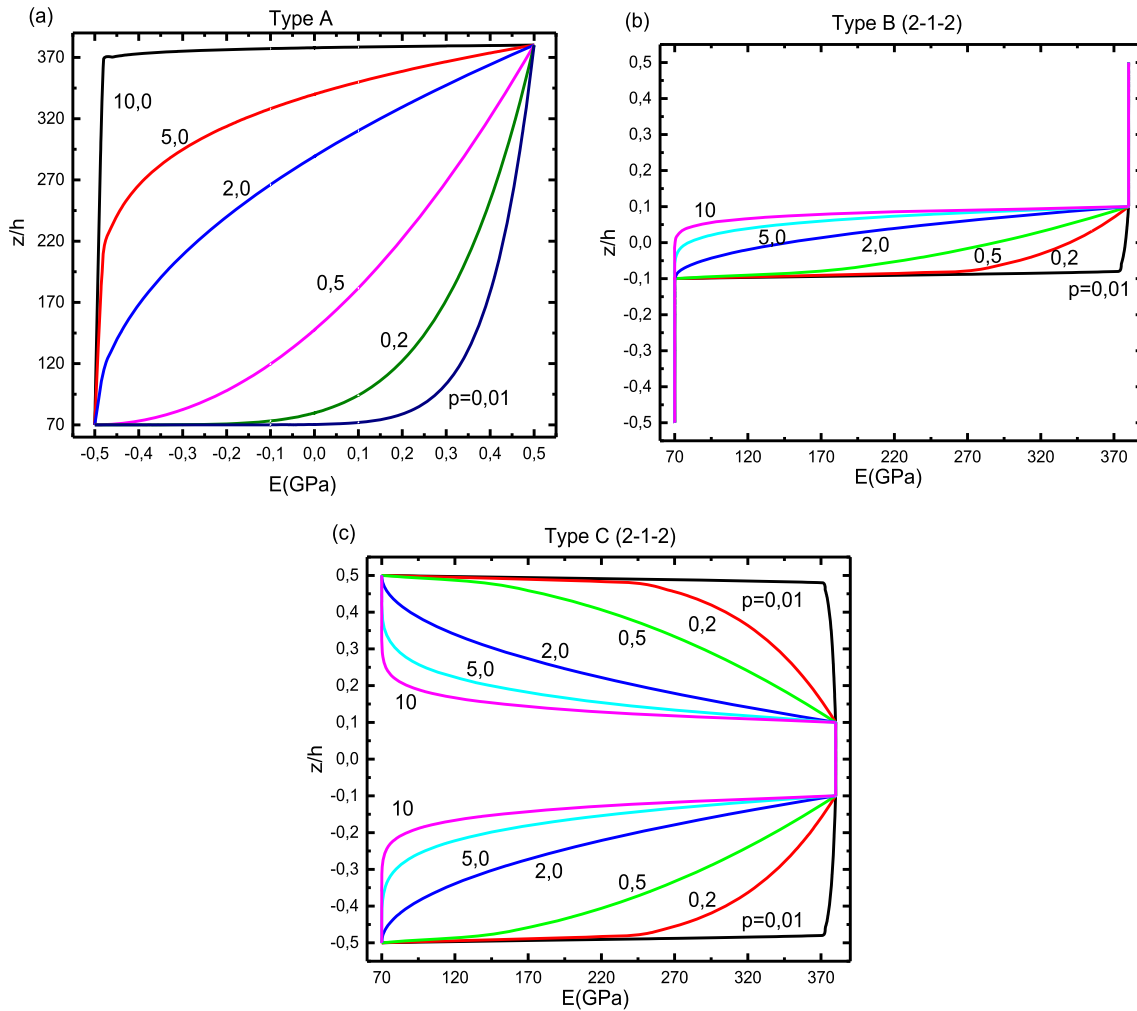


Fig. 2 Change of E across plate thickness of beams for different values of the power law index p : **a** Type A, **b** Type B (2-1-2), **c** Type C (2-1-2)

3 Numerical results and discussions

This section demonstrated the precision of the presented beam theory for bending analysis of isotropic and FG sandwich beams (FGSB) with different boundary conditions. This is done by comparing the analytical solution with previously published results in the literature. The study considers three types of functionally graded beams: A, B, and C.

The materials used in the combination are aluminum and alumina, each with specific material properties as follows:

Metal (Aluminum, Al): $E_m = 70$ GPa, $\nu_m = 0.3$.

Ceramic (Alumina, Al_2O_3): $E_c = 380$ GPa, $\nu_c = 0.3$.

In the following, it is noted that various types of sandwich beams are considered:

- (1-0-1) FGSB ($h_1 = h_2 = 0$): Plate consists of only two symmetrical and equally thick FG layers without a core layer.
- (1-1-1) FGSB ($h_1 = -h/6$, $h_2 = h/6$): Plate is symmetrical and consists of three equally thick layers.
- (2-1-1) FGSB ($h_1 = 0$, $h_2 = h/4$): Plate is nonsymmetric; the core thickness equals the upper face thickness, while it is half the lower face thickness.
- (2-1-2) FGSB ($h_1 = -h/10$, $h_2 = h/10$): Plate is symmetric.
- (1-2-1) FGSB ($h_1 = -h/4$, $h_2 = h/4$): Plate is symmetric.
- (2-2-1) FGSB ($h_1 = -h/10$, $h_2 = 3h/10$): Plate is nonsymmetric.

Table 4 Convergence studies for nondimensional deflection, fundamental frequency, and critical buckling load of FG beams (Type A) with $L/h = 5$ and $p = 1$

Boundary conditions	Number of series (m)								Vo et al. [62]
	2	4	6	8	10	12	14	16	
S-S	6.2820	6.2580	6.2599	6.2595	6.2596	6.2596	6.2596	6.2596	6.2594
C-F	57.0139	57.2873	57.3189	57.3267	57.3298	57.3310	57.3317	57.3323	57.3323
C-C	1.5999	1.6151	1.6171	1.6176	1.61775	1.6178	1.6179	1.6179	1.6179

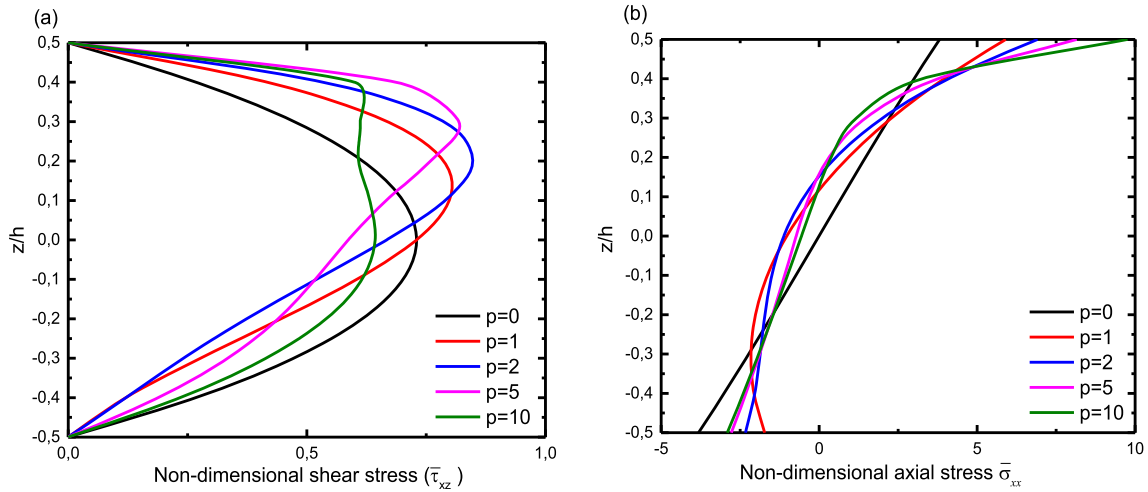

Fig. 3 Distribution of nondimensional stresses across the thickness of single layer FG (S-S) beam subjected to uniform load (Type A, $L/h = 5$)

Figure 2 indicates the across-the-thickness change in the modulus of elasticity (E) for $p = 0.01, 0.2, 0.5, 2, 5,$ and 10 for three types: (a) Type A, (b) Type B (2-1-2), and (c) Type C (2-1-2).

For ease of use, the following nondimensional form is utilized: the vertical displacement of beams subjected to a uniformly distributed load q :

$$\bar{w} = 100 \frac{E_m h^3}{q L^4} w \left(\frac{L}{2} \right) \text{ for S-S and C-C beams, } \bar{w} = 100 \frac{E_m h^3}{q L^4} w(L) \text{ for C-F beams}$$

$$\bar{\sigma}_x = \frac{h}{q L} \sigma_x \left(\frac{L}{2}, z \right), \quad \bar{\tau}_{xz} = \frac{h}{q L} \tau_{xz}(0, z).$$

3.1 Convergence study

The convergence studies analyzed the nondimensional deflections of FG beams (type A) with a uniform load q for different boundary conditions. The solutions were determined for the power law index ($p = 1$) and span-to-depth ratio ($L/h = 5$). It was observed that the solutions of the SS and CF beams converged more quickly than the CC beam. A sufficient number of terms ($m = 16$) were determined to acquire a precise solution, and this was used consistently throughout the numerical examples. Table 4, nondimensional deflections are compared with the results of Vo et al. [62] and good agreement is found (Fig. 3).

The research focused on studying the nondimensional deflections of FG beams (type A) with q for different boundary conditions. The analysis involved determining the solutions for $p = 1$ and $L/h = 5$. It was noted that the results of SS and CF beams demonstrated quicker convergence compared to the CC beam. To ensure precision, a sufficient number of terms ($m = 16$) were utilized consistently across the numerical examples.

Table 5 Comparison of the maximum vertical displacement of FG S–S beams (Type A) under a uniformly distributed load

L/h	BC	References	Model	$p = 0$	$p = 1$	$p = 2$	$p = 5$	$p = 10$
5	S–S	Present	Ritz	3.1668	6.2596	8.0689	9.8364	10.9173
		Li et al. [44]	HSDT	3.1657	6.2599	8.0602	9.7802	10.897
		Vo et al. [62]	Navier	3.1654	6.2594	8.0677	9.8281	10.938
		Vo et al. [62]	FE-TBT	3.1654	6.2590	8.0668	9.8271	10.937
20	S–S	Present	Ritz	2.8968	5.8059	7.4434	8.8203	9.6886
		Li et al. [44]	HSDT	2.8962	5.8049	7.4415	8.8151	9.6879
		Vo et al. [62]	Navier	2.8962	5.8049	7.4421	8.8182	9.6905
		Vo et al. [62]	FE-TBT	2.8963	5.8045	7.4412	8.8173	9.6899

Table 6 Comparison of $\bar{\sigma}_x$ of FG S–S beams (Type A)

L/h	References	Model	$p = 0$	$p = 1$	$p = 2$	$p = 5$	$p = 10$
5	Present	Ritz	3.8148	5.9053	6.9110	8.1522	9.7593
	Li et al. [44]	HSDT	3.8020	5.8837	6.8812	8.1030	9.7063
	Vo et al. [62]	Navier	3.8020	5.8836	6.8826	8.1106	9.7122
	Vo et al. [62]	FE-TBT	3.8040	5.8870	6.8860	8.1150	9.7170
20	Present	Ritz	15.0144	23.20814	27.1032	31.8199	38.1461
	Li et al. [59]	HSDT	15.0130	23.20542	27.0989	31.8112	38.1372
	Vo et al. [62]	Navier	15.0129	23.2053	27.0991	31.8130	38.1385
	Vo et al. [62]	FE-TBT	15.0200	23.2200	27.1100	31.8300	38.1600

Table 4 compares nondimensional deflections with the findings of Vo et al. [62], revealing a good agreement between the results.

3.2 FG beams (type A)

FG beams (Type A) under a uniformly distributed load are studied. The nondimensional transverse displacement (\bar{w}), axial stress ($\bar{\sigma}_x$), and transverse shear stress ($\bar{\tau}_{xz}$) obtained by using a recent refined hyperbolic shear deformation theory (RHSDT) for different boundary conditions are demonstrated in Tables 5, 6, 7 and 8. The results attained are compared with solutions reported by Li et al. [44] and Vo et al. [62]. It can be observed that the values obtained using a recent RHSDT are in good agreement with those given by Li et al. [44] and Vo et al. [62] for all values of p and L/h . Tables 5 and 6 indicate that the results obtained using the Ritz method closely align with those of Li et al. [44] and Vo et al. [62], particularly with regard to normal stress and vertical displacement. The current findings are consistent with prior studies, affirming the accuracy of the current model. The relationship between shear strain parameters, slenderness ratio, and power law index for several boundary conditions is depicted in Figs. 4 and 5. Evidently, these parameters are affected by the slenderness ratio, the power law index, and boundary conditions, with a more pronounced effect observed for the C–F beams compared to the C–C beams and S–S. As the slenderness ratio increases, the nondimensional transverse displacement \bar{w} decreases (Fig. 5).

3.3 Sandwich beams with FG core and homogeneous faces

A bending analysis of Type B sandwich beams is conducted in this example. Tables 9, 10, and 11 display nondimensional \bar{w} , $\bar{\sigma}_x$ and $\bar{\tau}_{xz}$. These results have been compared with the solutions provided by Vo et al. [62], demonstrating a good agreement between the two results. The impact of the volume fraction index “ p ” on the variation of the nondimensional transverse displacement is depicted in Fig. 6 for both symmetric and nonsymmetrical square FG beams (Type B) with a side-to-thickness ratio of $L/h = 5$ and 20. Observing Fig. 6, it is evident that the \bar{w} increases rapidly from $p = 0$ to 0.5 and then continues to increase with further increments of p . In Fig. 7a, the graph illustrates the variations in $\bar{\tau}_{xz}$ throughout the thickness of FG sandwich beams.

Table 7 Comparison of $\bar{\tau}_{xz}$ of FG S–S beams (Type A)

L/h	References	Model	$p = 0$	$p = 1$	$p = 2$	$p = 5$	$p = 10$
5	Present	Ritz	0.7300	0.7300	0.6673	0.5869	0.6431
	Li et al. [59]	HSDT	0.7500	0.7500	0.6787	0.5790	0.6436
	Vo et al. [62]	Navier	0.7332	0.7332	0.6706	0.5905	0.6467
	Vo et al. [62]	FE-TBT	0.7335	0.7335	0.6700	0.5907	0.6477
20	Present	Ritz	0.7422	0.7422	0.6793	0.5987	0.6562
	Li et al. [44]	HSDT	0.7500	0.7500	0.6787	0.5790	0.6436
	Vo et al. [62]	Navier	0.7451	0.7451	0.6824	0.6023	0.6596
	Vo et al. [62]	FE-TBT	0.7470	0.7470	0.6777	0.6039	0.6682

Table 8 Maximum vertical displacement of FG (C–F) and FG (C–C) beams (Type A) under a uniformly distributed load

L/h	BC	References	Model	$p = 0$	$p = 1$	$p = 2$	$p = 5$	$p = 10$
5	C–C	Present	Ritz	0.8448	1.6179	2.1118	2.7386	3.1326
		Vo et al. [62]	FE-TBT	0.8501	1.6179	2.1151	2.7700	3.1812
	C–F	Present	Ritz	28.6857	57.3323	73.5830	87.7003	96.5137
		Vo et al. [62]	FE-TBT	28.7555	57.3323	73.6482	88.2044	97.4151
20	C–C	Present	Ritz	0.5902	1.1795	1.5139	1.8047	1.9856
		Vo et al. [62]	FE-TBT	0.5933	1.1843	1.5203	1.8155	2.0027
	C–F	Present	Ritz	27.6738	55.5073	71.1410	84.1661	92.4152
		Vo et al. [62]	FE-TBT	27.7029	55.5546	71.2051	84.2712	92.5571

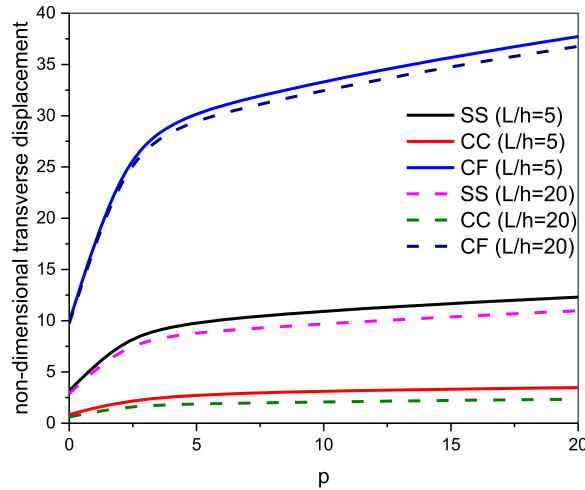


Fig. 4 Effects of the p on the nondimensional transverse displacement of FG beams (Type A, $L/h = 5$ and 20)

Unlike symmetric or homogeneous beams, the $\bar{\tau}_{xz}$ distribution for FG sandwich beams does not follow a parabolic pattern. It is worth noting that an increase in the value of p results in a decrease in transverse shear stress within the beam’s skin, potentially improving its resistance to face sheet debonding. Conversely, the homogeneous beam exhibits a peak of $\bar{\tau}_{xz}$ within the same region. In Fig. 7b, the $\bar{\sigma}_x$ is depicted as being tensile at the top surface and compressive at the bottom surface of the material. Additionally, the homogeneous beam is shown to experience the highest compressive stresses at its bottom surface and the lowest tensile stresses at its top surface. Moving on to Fig. 8, the graph illustrates the relationship between the nondimensional transverse displacement and the slenderness ratio of FG beams (Type B). It’s evident from the graph that the nondimensional transverse displacement significantly increases as the parameter “ p ” increases. This can be ascribed to the fact that E of ceramic material exceeds that of metal.

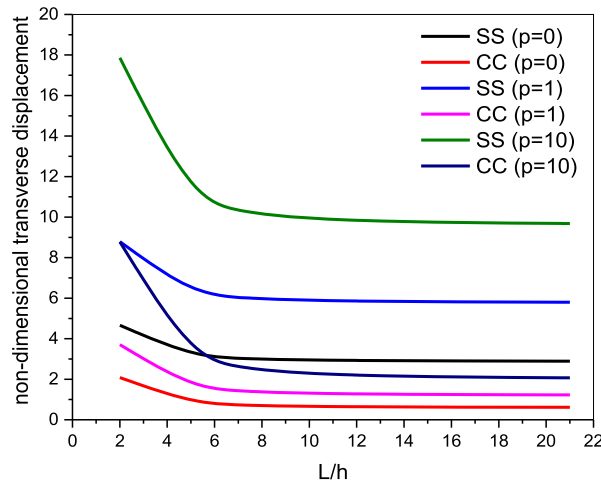


Fig. 5 Change of the nondimensional transverse displacement with respect to the slenderness ratio of FG beams (Type A)

Table 9 Maximum vertical displacement of (1–8–1) FGSB (Type B)

L/h	BC	References	Model	$p = 0$	$p = 1$	$p = 2$	$p = 5$	$p = 10$
5	S–S	Present	Ritz	3.9872	6.7307	8.0269	9.0958	9.5146
		Vo et al. [62]	Navier	3.9788	6.7166	8.0083	9.0691	9.4817
		Vo et al. [62]	FE-TBT	3.9788	6.7166	8.0083	9.0691	9.4817
	C–C	Present	Ritz	1.0244	1.7095	2.0783	2.5080	2.7353
		Vo et al. [62]	FE-TBT	1.0273	1.7079	2.0825	2.5386	2.7866
	C–F	Present	Ritz	35.9945	60.9929	72.2614	80.0466	83.3895
20	S–S	Vo et al. [62]	FE-TBT	36.4685	61.7373	73.2441	81.5334	84.2168
		Present	Ritz	3.6930	6.2638	7.4087	8.1595	8.3628
		Vo et al. [62]	Navier	3.6934	6.2638	7.4085	8.1587	8.3619
	C–C	Vo et al. [62]	FE-TBT	3.6934	6.2638	7.4085	8.1587	8.3619
		Present	Ritz	0.7486	1.2685	1.5030	1.6653	1.7143
	C–F	Vo et al. [62]	FE-TBT	0.7536	1.2759	1.5122	1.6784	1.7300
		Present	Ritz	35.3187	59.9199	70.8409	77.8944	79.7420
	Vo et al. [62]	FE-TBT	35.3495	59.9664	70.9018	77.9882	79.8588	

Table 10 Comparison of $\bar{\sigma}_x$ of (1–8–1) FG beams with S–S boundary conditions (Type B)

L/h	References	Model	$p = 0$	$p = 1$	$p = 2$	$p = 5$	$p = 10$
5	Present	Ritz	4.4795	6.0366	6.5312	6.9367	7.2764
	Vo et al. [62]	Navier	4.4636	6.0094	6.5256	6.8886	7.2229
	Vo et al. [62]	FE-TBT	4.4660	6.0130	6.5290	6.8930	7.2270
20	Present	Ritz	17.6373	23.7289	25.7156	27.0048	28.2638
	Vo et al. [62]	Navier	17.6327	23.7080	25.6849	26.9694	28.2283
	Vo et al. [62]	FE-TBT	17.6400	23.7200	25.7000	26.9800	28.2400

3.4 Sandwich beams with FG faces and homogeneous core (type C)

The analysis concludes by examining four types of sandwich beams of Type C: symmetric (1–1–1, 1–2–1) and nonsymmetric (2–1–1, 2–2–1). The vertical displacement for several boundary conditions is presented in Tables 12, 13 and 14 and visualized in Figs. 9 and 10. The obtained results from the analysis of symmetric and nonsymmetric sandwich beams are compared to the solutions provided by Vo et al. [62]. The results show strong agreement with the predictions based on Vo et al. [62]. Specifically, the smallest displacement

Table 11 Comparison of $\bar{\tau}_{xz}$ of (1–8–1) FG beams with S–S boundary conditions (TypeB)

L/h	Reference	Model	$p = 0$	$p = 1$	$p = 2$	$p = 5$	$p = 10$
5	Present	Ritz	0.7564	0.7287	0.6411	0.5280	0.5749
	Vo et al. [62]	Navier	0.7597	0.7318	0.6445	0.5319	0.5792
	Vo et al. [62]	FE-TBT	0.7611	0.7315	0.6432	0.5316	0.5798
20	Present	Ritz	0.7673	0.7408	0.6526	0.5387	0.5868
	Vo et al. [62]	Navier	0.7702	0.7436	0.6558	0.5425	0.5910
	Vo et al. [62]	FE-TBT	0.7785	0.7416	0.6452	0.5400	0.5969

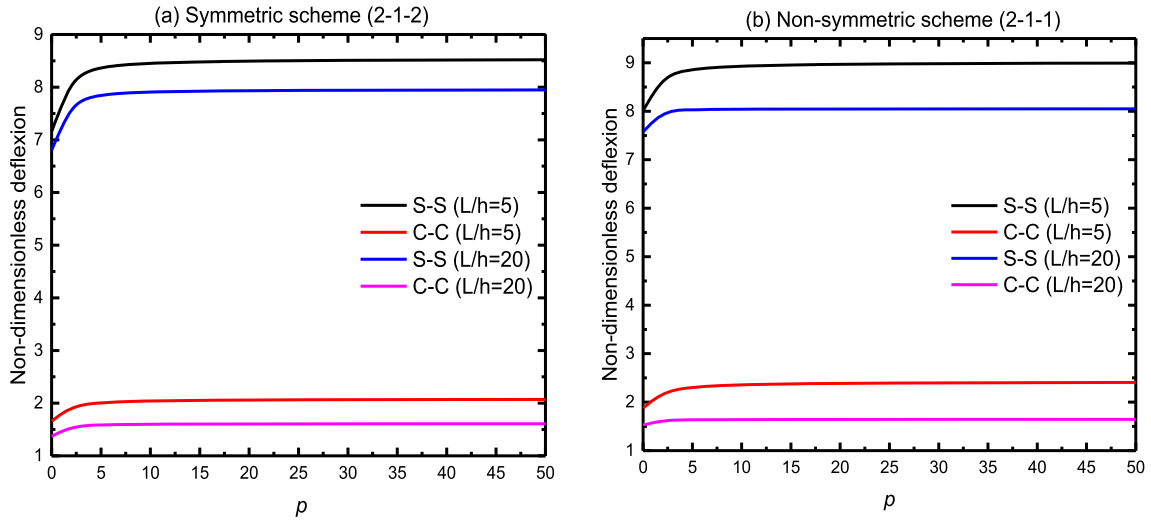


Fig. 6 Effects of the p on the nondimensional \bar{w} of FG beams (Type B, $L/h = 5$ and 20)

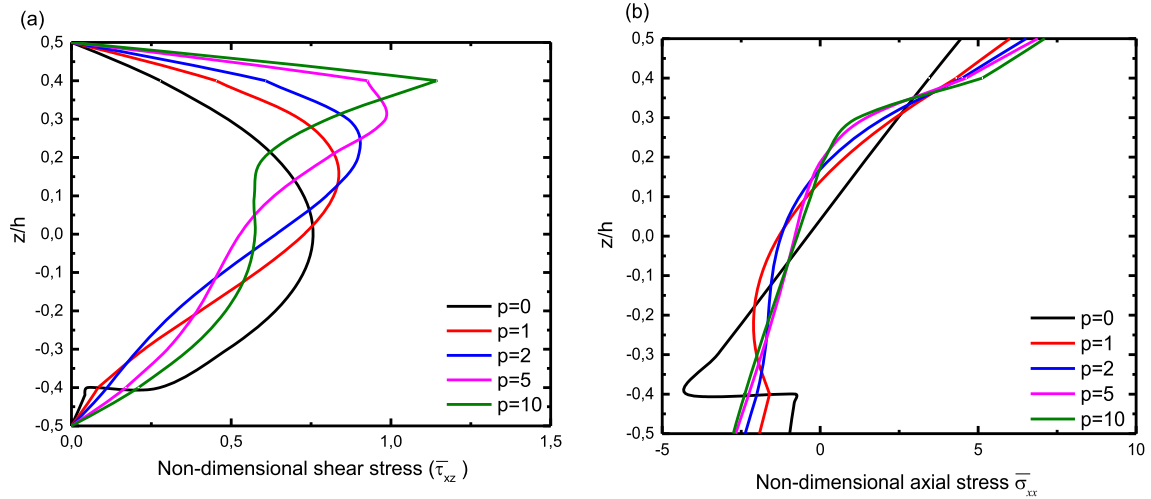


Fig. 7 Distribution of nondimensional stresses across the thickness of (1–8–1)FG sandwich S–S beams under uniform load (Type B, $L/h = 5$)

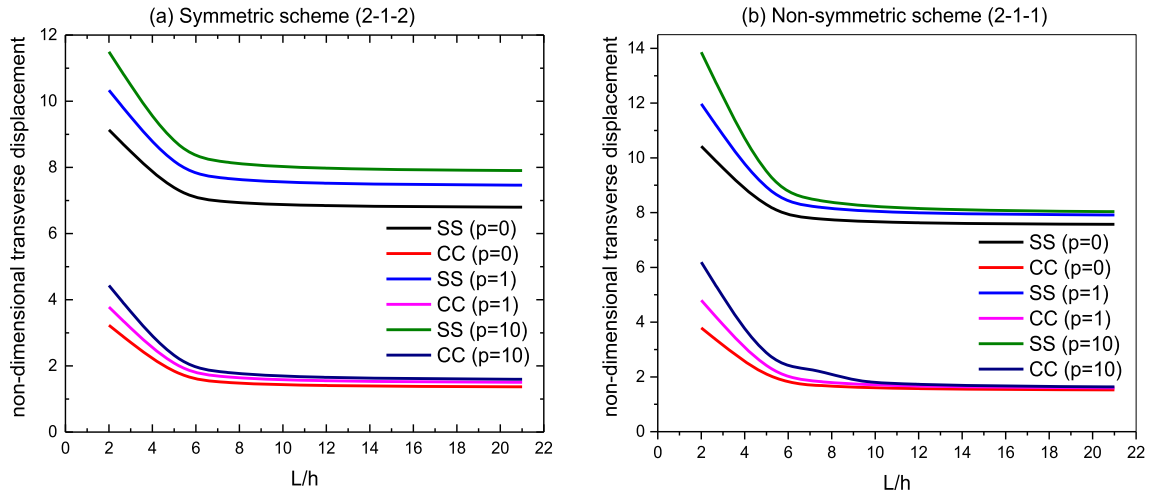


Fig. 8 Variation of the nondimensional \bar{w} with respect to the slenderness ratio of FG beams (Type B)

Table 12 Maximum vertical displacement of FGSB with S–S (Type C)

p	References	$L/h = 5$				$L/h = 20$			
		1–1–1	1–2–1	2–1–1	2–2–1	1–1–1	1–2–1	2–1–1	2–2–1
0	Present	3.1736	3.1736	3.1736	3.1736	2.8960	2.8960	2.8960	2.8960
	Vo et al. [62]	3.1654	3.1654	3.1654	3.1654	2.8963	2.8963	2.8963	2.8963
1	Present	6.2788	5.4212	6.5552	5.8498	5.9391	5.0999	6.1968	5.5153
	Vo et al. [62]	6.2693	5.4122	6.5450	5.8403	5.9401	5.1006	6.1977	5.5161
2	Present	8.3994	6.7671	8.9009	7.5683	8.0298	6.4265	8.4990	7.2069
	Vo et al. [62]	8.3893	6.7579	8.8896	7.5583	8.0313	6.4276	8.5003	7.2080
5	Present	11.2384	8.5238	11.8377	9.8028	10.8355	8.1627	11.3765	9.4106
	Vo et al. [62]	11.2274	8.5137	11.8246	9.7919	10.8376	8.1642	11.3782	9.4120
10	Present	12.1288	9.4147	13.0280	10.8601	12.1282	9.0454	12.5263	10.4510
	Vo et al. [62]	12.5659	9.4050	13.0135	10.8486	12.1593	9.0471	12.5281	10.4526

is observed in the (1–2–1) sandwich beam, while the largest displacement is found in the (2–1–1) sandwich beam. This discrepancy in displacement is attributed to the varying proportions of the ceramic phase in these beams compared to others.

Based on the information provided in the search results, the influence of the volume fraction index p on the nondimensional \bar{w} of FG beams is shown in Fig. 9 for both symmetric and unsymmetric square FG sandwich beams with side-to-thickness ratios $L/h = 5$ and 20. The key observations are:

The \bar{w} increases gradually as the volume fraction index p increases for symmetric and unsymmetric sandwich beams. The \bar{w} of the C–C FG sandwich beams is less than that of the simply supported FG sandwich beams. In other words, as the volume fraction index p increases, indicating a higher proportion of the ceramic phase, the transverse displacement of the FG sandwich beams increases. Additionally, the clamped–clamped boundary condition results in lower transverse displacement than the simply supported condition. Figure 10 displays the changes in the nondimensional \bar{w} for symmetric (2–1–2) and nonsymmetric scheme (2–1–1) versus the side-to-thickness ratio a/h for different values of the inhomogeneity parameter p . The nondimensional transverse displacement increases as p increases. The data in Tables 15 and 16 indicate that ceramic beams ($p = 0$) have the smallest of $\bar{\tau}_{xz}$ and the largest of $\bar{\sigma}_x$. As the power law index increases, the $\bar{\tau}_{xz}$ increases, while the $\bar{\sigma}_x$ decreases. The variations of these stresses across the thickness (h) are shown in Figs. 11 and 12. There are differences between the stresses of symmetric and nonsymmetric beams. Symmetric beams shown in Figs. 11a, b, 12a, and b exhibit the same maximum $\bar{\sigma}_x$ (tensile/compressive) at the core layer’s top/bottom surface. On the other hand, nonsymmetric beams demonstrate varying stress distributions. In nonsymmetric beams, the maximum tensile axial stress is located at the core layer’s top surface. In contrast, the maximum

Table 13 Maximum vertical displacement of FGSB with C–C (Type C)

p	References	$L/h = 5$				$L/h = 20$			
		1–1–1	1–2–1	2–1–1	2–2–1	1–1–1	1–2–1	2–1–1	2–2–1
0	Present	0.8506	0.8506	0.8506	0.8506	0.5902	0.5932	0.5932	0.5932
	Vo et al. [62]	0.8501	0.8501	0.8501	0.8501	0.5933	0.5933	0.5933	0.5933
1	Present	1.4682	1.2851	1.5934	1.4315	1.2014	1.0328	1.2537	1.1164
	Vo et al. [62]	1.5232	1.3372	1.5930	1.4332	1.2053	1.0365	1.2577	1.1202
2	Present	1.9111	1.5665	2.0966	1.8058	1.6208	1.2989	1.7159	1.4559
	Vo et al. [62]	1.9715	1.6225	2.0969	1.7988	1.6250	1.3028	1.7203	1.4599
5	Present	2.4998	1.9302	2.7574	2.2898	2.1834	1.6470	2.2939	1.8979
	Vo et al. [62]	2.5652	1.9896	2.7306	2.2700	2.1880	1.6512	2.2987	1.9021
10	Present	2.7788	2.1140	3.0304	2.5203	2.4484	1.8239	2.5255	2.1067
	Vo et al. [62]	2.8468	2.1747	3.0002	2.4945	2.4532	1.8282	2.5307	2.1110

Table 14 Maximum vertical displacement of FGSB with C–F (Type C)

p	References	$L/h = 5$				$L/h = 20$			
		1–1–1	1–2–1	2–1–1	2–2–1	1–1–1	1–2–1	2–1–1	2–2–1
0	Present	28.7531	28.7531	28.7531	28.7531	28.7531	28.7531	28.7531	28.7531
	Vo et al. [62]	28.7555	28.7555	28.7555	28.7555	28.7555	28.7555	28.7555	28.7555
1	Present	58.1640	50.0484	60.6949	53.5658	56.8651	48.8151	59.3307	52.7977
	Vo et al. [62]	58.1959	50.0741	60.7338	54.1078	56.9009	48.8489	59.3681	52.8327
2	Present	78.4754	62.9503	82.3394	69.8584	76.9268	61.5450	81.4168	69.0285
	Vo et al. [62]	78.3753	62.8813	82.9905	70.4450	76.9658	61.5809	81.4583	69.0661
5	Present	105.7203	79.8251	110.0781	91.0752	103.8525	78.2070	109.0192	90.1745
	Vo et al. [62]	105.4300	79.6213	110.8230	91.7109	103.8950	78.2451	109.0660	90.2148
10	Present	118.5202	88.4020	122.1920	101.0964	116.5322	86.6786	120.0402	100.1572
	Vo et al. [62]	118.1780	88.1270	122.0020	101.7590	116.5770	86.7178	120.0910	100.1990

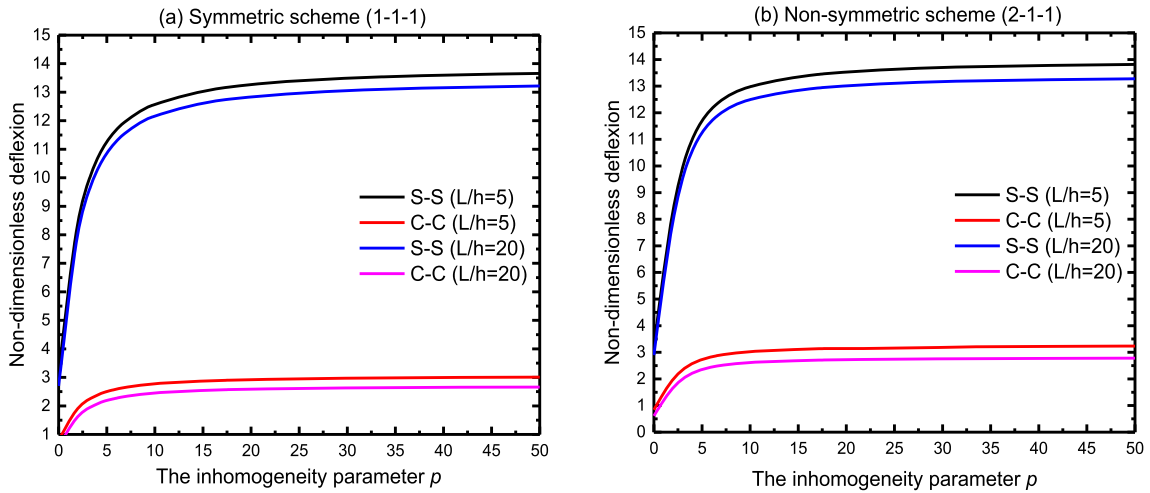


Fig. 9 Effects of the p on the nondimensional \bar{w} of FG beams (Type C, $L/h = 5$ and 20)

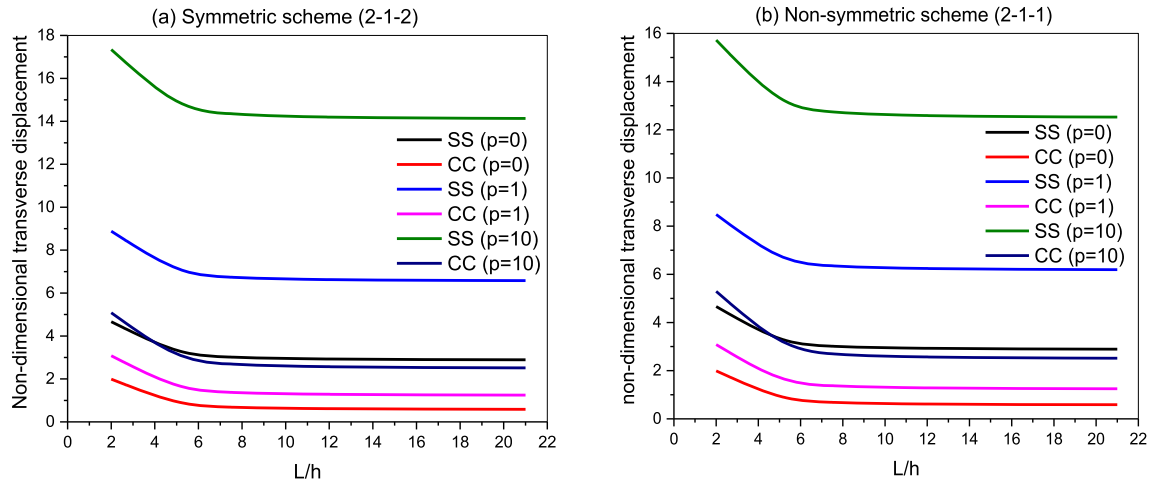


Fig. 10 Change of the nondimensional \bar{w} with respect to the side-to-thickness ratio of FG beams (Type C)

Table 15 Comparison of the axial stress $\bar{\sigma}_x$ o of FG beams with S-S (Type C)

p	References	L/h = 5				L/h = 20			
		1-1-1	1-2-1	2-1-1	2-2-1	1-1-1	1-2-1	2-1-1	2-2-1
0	Present	3.8154	3.8154	3.8154	3.8154	15.0146	15.0146	15.0146	15.0146
	Vo et al. [62]	3.8020	3.8020	3.8020	3.8020	15.0129	15.0129	15.0129	15.0129
1	Present	1.4385	1.2364	1.3878	1.2462	5.6852	4.8804	5.4963	4.9367
	Vo et al. [62]	1.4349	1.2329	1.3884	1.2474	5.6850	4.8801	5.4960	4.9364
2	Present	1.9377	1.5567	1.8474	1.5862	7.6913	6.1535	7.3230	6.2892
	Vo et al. [62]	1.9382	1.5527	1.8475	1.5873	7.6912	6.1532	7.3227	6.2889
5	Present	2.6120	1.9748	2.4083	2.0189	10.3835	7.8196	9.5510	8.0110
	Vo et al. [62]	2.6123	1.9705	2.4069	2.0194	10.3835	7.8194	9.5508	8.0109
10	Present	2.9261	2.1869	2.6294	2.2199	11.6510	8.6666	10.4359	8.8105
	Vo et al. [62]	2.9293	2.1826	2.6296	2.2199	11.6513	8.6665	10.4357	8.8104

compressive of $\bar{\sigma}_x$ is found at the core layer’s bottom surface. Furthermore, it’s worth noting that regardless of beam symmetry, the maximum value of $\bar{\tau}_{xz}$ occurs at the midplane of the beam, as illustrated in Fig. 12.

4 Conclusions

This study presents a recent refined hyperbolic shear deformation theory (RHSDT) for analyzing the mechanical behavior of both isotropic and sandwich functionally graded material (FGM) beams. The proposed theory incorporates a novel hyperbolic distribution of transverse shear stress and satisfies the traction-free boundary conditions. Analytical trigonometric series solutions are derived for three types of FG beams under various boundary conditions. Various types of symmetric and nonsymmetric sandwich beams are considered. Numerical results are presented for different boundary conditions to investigate the effects of length-to-depth ratio, boundary conditions, power law index, and skin–core–skin thickness ratios and configurations on the structural response of the isotropic and sandwich functionally graded beams. The findings highlight the accuracy and efficiency of the RHSDT in predicting the mechanical behavior of FGM beams. The study also underscores the importance of considering various boundary conditions and geometric configurations in the design and analysis of FGM beams. Future research directions, such as those outlined by Tounsi et al. [108] on the wave propagation characteristics of functionally graded porous shells, could further enhance the understanding and application of RHSDT in analyzing more complex structural components.

Table 16 Comparison of the shear stress $\bar{\tau}_{xz}$ of FG beams with S–S boundary conditions (Type C)

p	References	$L/h = 5$				$L/h = 20$			
		1–1–1	1–2–1	2–1–1	2–2–1	1–1–1	1–2–1	2–1–1	2–2–1
0	Present	0.7300	0.7300	0.7300	0.7300	0.7422	0.7422	0.7422	0.7422
	Vo et al. [62]	0.7332	0.7332	0.7332	0.7332	0.7451	0.7451	0.7451	0.7451
1	Present	0.8557	0.8091	0.9058	0.8449	0.8660	0.8189	0.9167	0.8551
	Vo et al. [62]	0.8586	0.8123	0.9088	0.8479	0.8681	0.8215	0.9191	0.8575
2	Present	0.9225	0.8463	1.0109	0.9047	0.9328	0.8557	1.0222	0.9147
	Vo et al. [62]	0.9249	0.8493	1.0136	0.9075	0.9344	0.8581	1.0242	0.9168
5	Present	1.0111	0.8898	1.1719	0.9836	1.0223	0.8995	1.1849	0.9942
	Vo et al. [62]	1.0125	0.8925	1.1742	0.9859	1.0227	0.9014	1.1862	0.9957
10	Present	1.0658	0.9128	1.2854	1.0314	1.0775	0.9228	1.2997	1.0425
	Vo et al. [62]	1.0665	0.9151	1.2875	1.0335	1.0773	0.9243	1.3008	1.0436

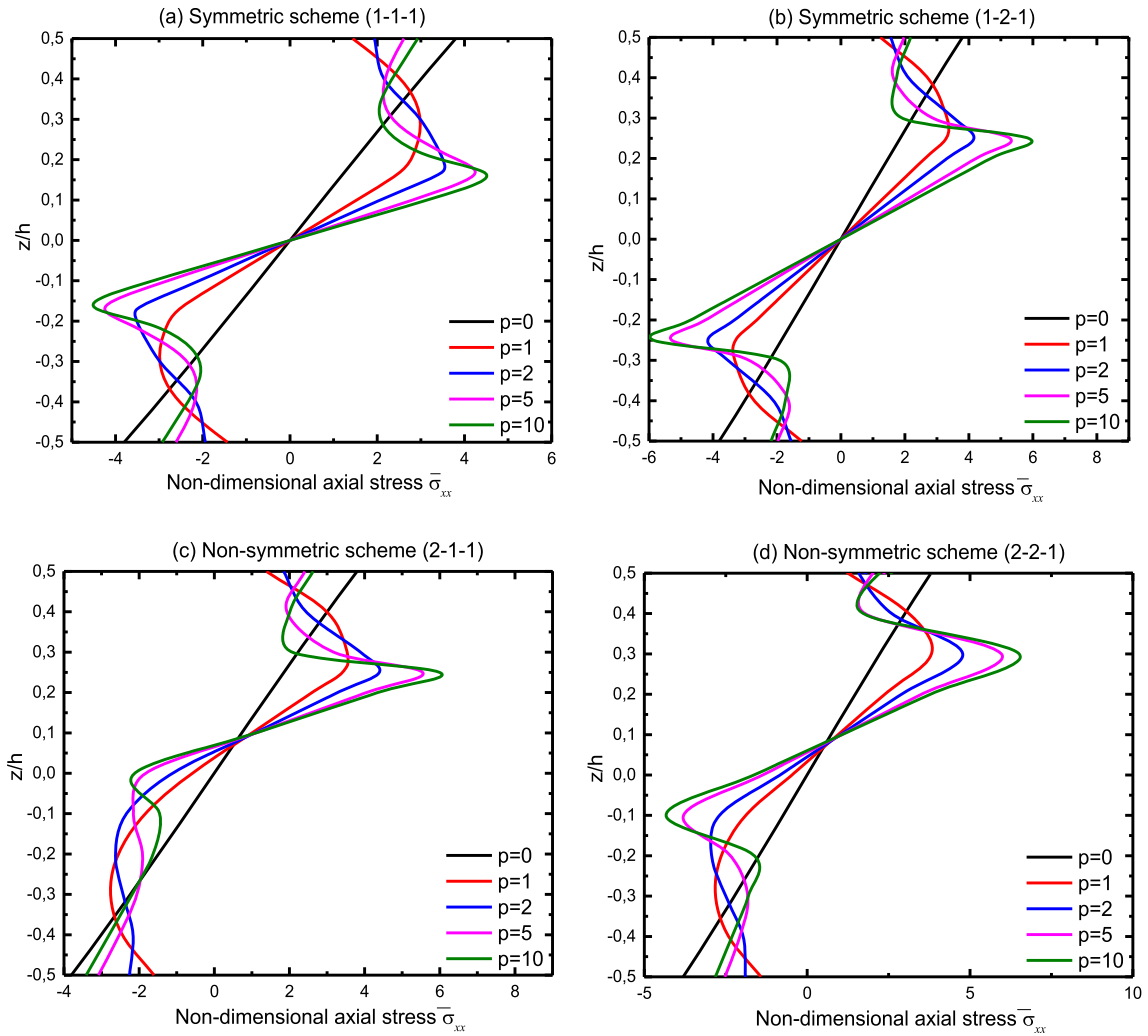


Fig. 11 Distribution of nondimensional stresses across the thickness of FG sandwich S–S beams subjected to uniform load (Type C, $L/h = 5$)

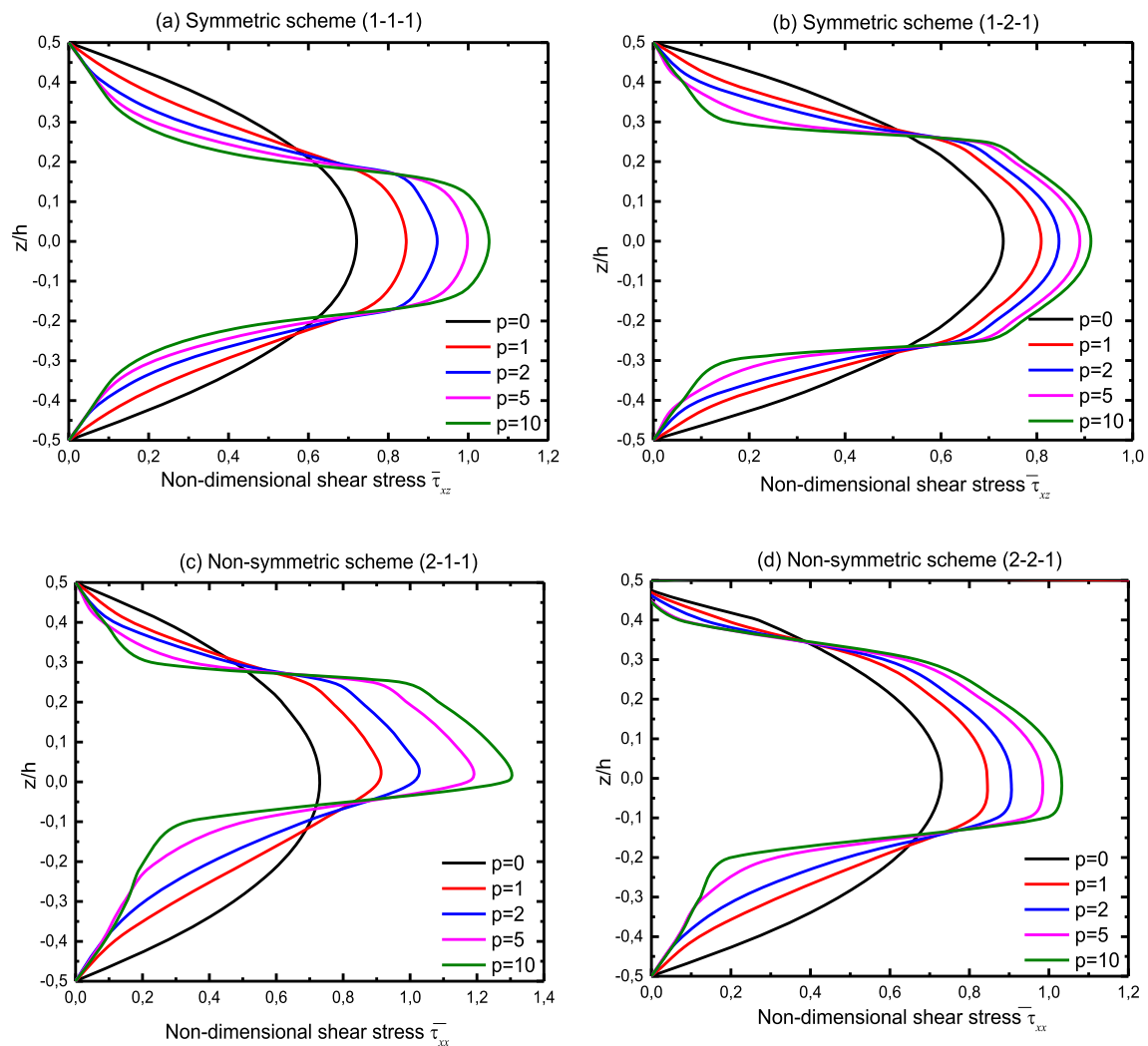


Fig. 12 Distribution of nondimensional shear stresses across the thickness of FG sandwich S-S beams subjected to uniform load (Type C, $L = h = 5$)

Acknowledgements The authors extend their appreciation to Taif University, Saudi Arabia, for supporting this work through project number (TU-DSPP-2024-66).

Data availability No data associated in the manuscript.

Declarations

Conflict of interest The authors declare no conflict of interest in preparing this article.

References

1. Koizumi, M.: The concept of FGM ceramic transactions. *Funct. Gradient Mater.* **34**, 3–10 (1993)
2. Koizumi, M.: FGM activities in Japan. *Compos. B Eng.* **28**(1–2), 1–4 (1997). [https://doi.org/10.1016/S1359-8368\(96\)00016-9](https://doi.org/10.1016/S1359-8368(96)00016-9)
3. Suresh, S., Mortensen, A.: *Fundamentals of Functionally Graded Materials*. IOM Commun. Ltd, Cambridge (1998)
4. Miyamoto, Y., Kaysner, W.A., Rabin, B.H., Kawasaki, A., Ford, R.G. (eds.): *Functionally Graded Materials: Design, Processing and Applications*, vol. 5. Springer, Berlin (2013)

5. Matsuo, S., Watari, F., Ohata, N.: Fabrication of a functionally graded dental composite resin post and core by laser lithography and finite element analysis of its stress relaxation effect on tooth root. *Dent. Mater. J.* **20**(4), 257–274 (2001). <https://doi.org/10.4012/DMJ.20.257>
6. Pompe, W., Worch, H., Epple, M., Friess, W., Gelinsky, M., Greil, P., Hempel, U., Scharnweber, D., Schulte, K.: Functionally graded materials for biomedical applications. *Mater. Sci. Eng. A* **362**(1–2), 40–60 (2003). [https://doi.org/10.1016/S0921-5093\(03\)00580-X](https://doi.org/10.1016/S0921-5093(03)00580-X)
7. Watari, F., Yokoyama, A., Omori, M., Hirai, T., Kondo, H., Uo, M., Kawasaki, T.: Biocompatibility of materials and development to functionally graded implant for biomedical application. *Compos. Sci. Technol.* **64**(6), 893–908 (2004). <https://doi.org/10.1016/j.compscitech.2003.09.025>
8. Mueller, E., Drašar, Č., Schilz, J., Kaysser, W.A.: Functionally graded materials for sensor and energy applications. *Mater. Sci. Eng. A* **362**(1–2), 17–39 (2003). [https://doi.org/10.1016/S0921-5093\(03\)00581-1](https://doi.org/10.1016/S0921-5093(03)00581-1)
9. Radhi, N.S.: Preparation and modeling (titanium-hydroxyapatite) functionally graded materials for bio-medical application. *Int. J. Civ. Eng. Technol. IJCIET* **9**(6), 28–39 (2018)
10. Radhi, N., Hafiz, M., Atiyah, A.: Preparation and investigation of corrosion and biocompatibility properties for functionally graded materials (NiTi). *Ind. Eng. Manag. S* **3**, 2169–2316 (2018). <https://doi.org/10.4172/2169-0316.100030>
11. Zhang, B., Jaiswal, P., Rai, R., Nelaturi, S.: Additive manufacturing of functionally graded material objects: a review. *J. Comput. Inf. Sci. Eng.* **18**(4), 041002 (2018). <https://doi.org/10.1115/1.4040705>
12. Dabbagh, A., Madfa, A., Naderi, S., Talaeizadeh, M., Abdullah, H., Abdulmunem, M., Kasim, N.A.: Thermomechanical advantages of functionally graded dental posts: a finite element analysis. *Mech. Adv. Mater. Struct.* **26**(8), 700–709 (2019). <https://doi.org/10.1080/15376494.2017.1410909>
13. Mahmoudi, M., Saidi, A.R., Hashemipour, M.A., Amini, P.: The use of functionally graded dental crowns to improve biocompatibility: a finite element analysis. *Comput. Methods Biomech. Biomed. Engin.* **21**(2), 161–168 (2018). <https://doi.org/10.1080/10255842.2018.1431219>
14. Patil, V., Naik, N., Gadicherla, S., Smriti, K., Raju, A., Rathee, U.: Biomechanical behavior of bioactive material in dental implant: a three-dimensional finite element analysis. *Sci. World J.* **2020**, 1 (2020). <https://doi.org/10.1155/2020/2363298>
15. Saleh, B., Jiang, J., Fathi, R., Al-hababi, T., Xu, Q., Wang, L., Song, D., Ma, A.: 30 Years of functionally graded materials: An overview of manufacturing methods, applications and future challenges. *Compos. Part B Eng.* **201**, 108376 (2020). <https://doi.org/10.1016/j.compositesb.2020.108376>
16. Miteva, A., Bouzekova-Penkova, A.: Some aerospace applications of functionally graded materials. *Aerosp. Res. Bulg* **33**, 195–209 (2021). <https://doi.org/10.3897/arb.v33.e14>
17. Sankar, B.V.: An elasticity solution for functionally graded beams. *Compos. Sci. Technol.* **61**(5), 689–696 (2001). [https://doi.org/10.1016/S0266-3538\(01\)00007-0](https://doi.org/10.1016/S0266-3538(01)00007-0)
18. Sankar, B.V., Tzeng, J.T.: Thermal stresses in functionally graded beams. *AIAA J.* **40**(6), 1228–1232 (2002). <https://doi.org/10.2514/2.1783>
19. Zhong, Z., Yu, T.: Analytical solution of a cantilever functionally graded beam. *Compos. Sci. Technol.* **67**(3–4), 481–488 (2007). <https://doi.org/10.1016/j.compscitech.2006.08.023>
20. Ding, H.J., Huang, D.J., Chen, W.: Elasticity solutions for plane anisotropic functionally graded beams. *Int. J. Solids Struct.* **44**(1), 176–196 (2007). <https://doi.org/10.1016/j.ijsolstr.2006.04.026>
21. Huang, D.J., Ding, H.J., Chen, W.Q.: Analytical solution for functionally graded anisotropic cantilever beam subjected to linearly distributed load. *Appl. Math. Mech.* **28**(7), 855–860 (2007). <https://doi.org/10.1007/s10483-007-0702-1>
22. Ying, J., Lü, C.F., Chen, W.Q.: Two-dimensional elasticity solutions for functionally graded beams resting on elastic foundations. *Compos. Struct.* **84**(3), 209–219 (2008). <https://doi.org/10.1016/j.compstruct.2007.07.004>
23. Yang, Q., Zheng, B., Zhang, K., Zhu, J.: Analytical solution of a bilayer functionally graded cantilever beam with concentrated loads. *Arch. Appl. Mech.* **83**, 455–466 (2013). <https://doi.org/10.1007/s00419-012-0667-0>
24. Xu, Y., Yu, T., Zhou, D.: Two-dimensional elasticity solution for bending of functionally graded beams with variable thickness. *Meccanica* **49**, 2479–2489 (2014). <https://doi.org/10.1007/s11012-014-9998-7>
25. Celebi, K., Tutuncu, N.: Free vibration analysis of functionally graded beams using an exact plane elasticity approach. *Proc. Inst. Mech. Eng. C J. Mech. Eng. Sci.* **228**(14), 2488–2494 (2014). <https://doi.org/10.1177/0954406213519974>
26. Chu, P., Li, X.F., Wu, J.X., Lee, K.: Two-dimensional elasticity solution of elastic strips and beams made of functionally graded materials under tension and bending. *Acta Mech.* **226**, 2235–2253 (2015). <https://doi.org/10.1007/s00707-014-1294-y>
27. Pradhan, K.K., Chakraverty, S.: Free vibration of functionally graded thin elliptic plates with various edge supports. *Struct. Eng. Mech.* **53**(2), 337–354 (2015). <https://doi.org/10.12989/sem.2015.53.2.337>
28. Arefi, M.: The effect of different functionalities of FGM and FGPM layers on free vibration analysis of the FG circular plates integrated with piezoelectric layers. *Smart Struct. Syst.* **15**(5), 1345–1362 (2015). <https://doi.org/10.12989/sss.2015.15.5.1345>
29. Darilmaz, K.: Vibration analysis of functionally graded material (FGM) grid systems. *Steel Compos. Struct.* **18**(2), 395–408 (2015). <https://doi.org/10.12989/scs.2015.18.2.395>
30. Abrate, S.: Functionally graded plates behave like homogeneous plates. *Compos. B Eng.* **39**(1), 151–158 (2008). <https://doi.org/10.1016/j.compositesb.2007.02.026>
31. Zhang, D.G., Zhou, Y.H.: A theoretical analysis of FGM thin plates based on physical neutral surface. *Comput. Mater. Sci.* **44**(2), 716–720 (2008). <https://doi.org/10.1016/j.commatsci.2008.05.006>
32. Woo, J., Meguid, S.A., Ong, L.S.: Nonlinear free vibration behavior of functionally graded plates. *J. Sound Vib.* **289**(3), 595–611 (2006). <https://doi.org/10.1016/j.jsv.2005.03.029>
33. Duc, N.D., Seung-Eock, K., Chan, D.Q.: Thermal buckling analysis of FGM sandwich truncated conical shells reinforced by FGM stiffeners resting on elastic foundations using FSDT. *J. Therm. Stress.* **41**(3), 331–365 (2018). <https://doi.org/10.1080/01495739.2017.1398623>
34. Wei, D., Liu, Y., Xiang, Z.: An analytical method for free vibration analysis of functionally graded beams with edge cracks. *J. Sound Vib.* **331**(7), 1686–1700 (2012). <https://doi.org/10.1016/j.jsv.2011.11.012>

35. Sina, S.A., Navazi, H.M., Haddadpour, H.: An analytical method for free vibration analysis of functionally graded beams. *Mater. Des.* **30**(3), 741–747 (2009). <https://doi.org/10.1016/j.matdes.2008.05.015>
36. Shanab, R.A., Attia, M.A.: On bending, buckling and free vibration analysis of 2D-FG tapered Timoshenko nanobeams based on modified couple stress and surface energy theories. *Waves Random Complex Media* **33**(3), 590–636 (2023). <https://doi.org/10.1080/17455030.2022.2105885>
37. Li, X.F.: A unified approach for analyzing static and dynamic behaviors of functionally graded Timoshenko and Euler–Bernoulli beams. *J. Sound Vib.* **318**(4–5), 1210–1229 (2008). <https://doi.org/10.1016/j.jsv.2008.04.056>
38. Chakraborty, A., Gopalakrishnan, S., Reddy, J.: A new beam finite element for the analysis of functionally graded materials. *Int. J. Mech. Sci.* **45**(3), 519–539 (2003). [https://doi.org/10.1016/S0020-7403\(03\)00058-4](https://doi.org/10.1016/S0020-7403(03)00058-4)
39. Boutahar, Y., Lebaal, N., Bassir, D.: A refined theory for bending vibratory analysis of thick functionally graded beams. *Mathematics* **9**(12), 1422 (2021). <https://doi.org/10.3390/math9121422>
40. Srividhya, S., Raghu, P., Rajagopal, A., Reddy, J.: Nonlocal nonlinear analysis of functionally graded plates using third-order shear deformation theory. *Int. J. Eng. Sci.* **125**, 1–22 (2018). <https://doi.org/10.1016/j.ijengsci.2018.10.004>
41. Wattanasakulpong, N., Prusty, B.G., Kelly, D.W.: Thermal buckling and elastic vibration of third-order shear deformable functionally graded beams. *Int. J. Mech. Sci.* **53**(9), 734–743 (2011). <https://doi.org/10.1016/j.ijmecsci.2011.05.003>
42. Carrera, E., Giunta, G., Petrolo, M.: *Beam Structures: Classical and Advanced Theories*. Wiley, Hoboken (2011)
43. Şimşek, M.: Fundamental frequency analysis of functionally graded beams by using different higher-order beam theories. *Nucl. Eng. Des.* **240**(4), 697–705 (2010). <https://doi.org/10.1016/j.nucengdes.2010.01.011>
44. Li, X.F., Wang, B.L., Han, J.C.: A higher-order theory for static and dynamic analyses of functionally graded beams. *Arch. Appl. Mech.* **80**, 1197–1212 (2010). <https://doi.org/10.1007/s00419-010-0435-6>
45. Karama, M., Afaq, K.S., Mistou, S.: Mechanical behaviour of laminated composite beam by the new multi-layered laminated composite structures model with transverse shear stress continuity. *Int. J. Solids Struct.* **40**(6), 1525–1546 (2003). [https://doi.org/10.1016/S0020-7683\(02\)00647-9](https://doi.org/10.1016/S0020-7683(02)00647-9)
46. Sayyad, A.S., Ghugal, Y.M.: Bending, buckling and free vibration analysis of size-dependent nanoscale FG beams using refined models and Eringen’s nonlocal theory. *Int. J. Appl. Mech.* **12**(01), 2050007 (2020). <https://doi.org/10.1142/S1758825120500075>
47. Soldatos, K.: A transverse shear deformation theory for homogeneous monoclinic plates. *Acta Mech.* **94**(3), 195–220 (1992). <https://doi.org/10.1007/BF01170621>
48. Carrera, E.: Theories and finite elements for multilayered plates and shells: a unified compact formulation with numerical assessment and benchmarking. *Arch. Comput. Methods Eng.* **10**, 215–296 (2003). <https://doi.org/10.1007/BF02736224>
49. Touratier, M.: An efficient standard plate theory. *Int. J. Eng. Sci.* **29**(8), 901–916 (1991). [https://doi.org/10.1016/0020-7225\(91\)90165-F](https://doi.org/10.1016/0020-7225(91)90165-F)
50. Reddy, J.N.: A simple higher-order theory for laminated composite plates. *J. Appl. Mech.* **51**(4), 745–752 (1984). <https://doi.org/10.1115/1.3167719>
51. Zhao, Y., Huang, Y., Guo, M.: A novel approach for free vibration of axially functionally graded beams with non-uniform cross-section based on Chebyshev polynomials theory. *Compos. Struct.* **168**, 277–284 (2017). <https://doi.org/10.1016/j.compstruct.2017.02.012>
52. Kahya, V., Turan, M.: Finite element model for vibration and buckling of functionally graded beams based on the first-order shear deformation theory. *Compos. B Eng.* **109**, 108–115 (2017). <https://doi.org/10.1016/j.compositesb.2016.10.039>
53. Parashar, S.K., Sharma, P.: Modal analysis of shear-induced flexural vibration of FGPM beam using generalized differential quadrature method. *Compos. Struct.* **139**, 222–232 (2016). <https://doi.org/10.1016/j.compstruct.2015.12.012>
54. Frikha, A., Hajlaoui, A., Wali, M., Dammak, F.: A new higher order C0 mixed beam element for FGM beams analysis. *Compos. B Eng.* **106**, 181–189 (2016). <https://doi.org/10.1016/j.compositesb.2016.09.024>
55. Jing, L.L., Ming, P.J., Zhang, W.P., Fu, L.R., Cao, Y.P.: Static and free vibration analysis of functionally graded beams by combination Timoshenko theory and finite volume method. *Compos. Struct.* **138**, 192–213 (2016). <https://doi.org/10.1016/j.compstruct.2015.11.027>
56. Yang, Y., Lam, C.C., Kou, K.P.: Forced vibration analysis of functionally graded beams by the meshfree boundary-domain integral equation method. *Eng. Anal. Bound. Elem.* **72**, 100–110 (2016). <https://doi.org/10.1016/j.enganabound.2016.07.010>
57. Şimşek, M.: Buckling of Timoshenko beams composed of two-dimensional functionally graded material (2D-FGM) having different boundary conditions. *Compos. Struct.* **149**, 304–314 (2016). <https://doi.org/10.1016/j.compstruct.2016.04.026>
58. Zahedinejad, P.: Free vibration analysis of functionally graded beams resting on elastic foundation in thermal environment. *Int. J. Struct. Stab. Dyn.* **16**(07), 1550029 (2016). <https://doi.org/10.1142/S0219455415500292>
59. Wattanasakulpong, N., Chaikittiratana, A.: Flexural vibration of imperfect functionally graded beams based on Timoshenko beam theory: Chebyshev collocation method. *Meccanica* **50**, 1331–1342 (2015). <https://doi.org/10.1007/s11012-015-0101-7>
60. Wattanasakulpong, N., Mao, Q.: Dynamic response of Timoshenko functionally graded beams with classical and non-classical boundary conditions using Chebyshev collocation method. *Compos. Struct.* **119**, 346–354 (2015). <https://doi.org/10.1016/j.compstruct.2014.08.031>
61. Jin, C., Wang, X.: Accurate free vibration analysis of Euler functionally graded beams by the weak form quadrature element method. *Compos. Struct.* **125**, 41–50 (2015). <https://doi.org/10.1016/j.compstruct.2015.01.039>
62. Vo, T.P., Thai, H.T., Nguyen, T.K., Inam, F.: Static and vibration analysis of functionally graded beams using refined shear deformation theory. *Meccanica* **49**, 155–168 (2014). <https://doi.org/10.1007/s11012-013-9806-y>
63. Pradhan, K.K., Chakraverty, S.: Free vibration of Euler and Timoshenko functionally graded beams by Rayleigh–Ritz method. *Compos. B Eng.* **51**, 175–184 (2013). <https://doi.org/10.1016/j.compositesb.2013.02.027>
64. Mohanty, S.C., Dash, R.R., Rout, T.: Static and dynamic stability analysis of a functionally graded Timoshenko beam. *Int. J. Struct. Stab. Dyn.* **12**(04), 1250025 (2012). <https://doi.org/10.1142/S0219455412500253>
65. Khalili, S.M.R., Jafari, A.A., Eftekhari, S.A.: A mixed Ritz-DQ method for forced vibration of functionally graded beams carrying moving loads. *Compos. Struct.* **92**(10), 2497–2511 (2010). <https://doi.org/10.1016/j.compstruct.2010.02.012>

66. Şimşek, M.: Static analysis of a functionally graded beam under a uniformly distributed load by Ritz method. *Int. J. Eng. Appl. Sci.* **1**(3), 1–11 (2009)
67. Arefi, M., Najafitabar, F.: Buckling and free vibration analyses of a sandwich beam made of a soft core with FG-GNPs reinforced composite face-sheets using Ritz method. *Thin Walled Struct.* **158**, 107200 (2021). <https://doi.org/10.1016/j.tws.2020.107200>
68. Chakraborty, A., Gopalakrishnan, S.: A spectrally formulated finite element for wave propagation analysis in functionally graded beams. *Int. J. Solids Struct.* **40**(10), 2421–2448 (2003). [https://doi.org/10.1016/S0020-7683\(03\)00029-5](https://doi.org/10.1016/S0020-7683(03)00029-5)
69. Jena, S.K., Chakraverty, S., Malikan, M.: Application of shifted Chebyshev polynomial-based Rayleigh–Ritz method and Navier’s technique for vibration analysis of a functionally graded porous beam embedded in Kerr foundation. *Eng. Comput.* **37**, 3569–3589 (2021). <https://doi.org/10.1007/s00366-020-01018-7>
70. Zhang, S., He, Y., Fan, L., Chen, X.: Active vibration control of smart beam by μ -synthesis technology: modeling via finite element method based on FSDT. *Mech. Adv. Mater. Struct.* **30**(22), 4671–4684 (2023). <https://doi.org/10.1080/15376494.2022.1234567>
71. Uzun, B., Yaylı, M.Ö., Deliktaş, B.: Free vibration of FG nanobeam using a finite element method. *Micro Nano Lett.* **15**(1), 35–40 (2020). <https://doi.org/10.1049/mnl.2019.0126>
72. Neamah, R.A., Nassar, A.A., Alansari, L.S.: Buckling simulation of simply support FG beam based on different beam theories. *Basrah J. Eng. Sci.* **21**(3), 10–24 (2021). <https://doi.org/10.33971/bjes.21.3.2>
73. Pang, F., Gao, C., Li, H., Jia, D., Wang, X., Miao, X.: Vibration analysis of FG beams under arbitrary load with general boundary conditions: theoretical and experimental comparative research. *Thin Walled Struct.* **179**, 109605 (2022). <https://doi.org/10.1016/j.tws.2022.109605>
74. Xu, J., Yang, Z., Yang, J., Li, Y.: Free vibration analysis of rotating FG-CNT reinforced composite beams in thermal environments with general boundary conditions. *Aerosp. Sci. Technol.* **118**, 107030 (2021). <https://doi.org/10.1016/j.ast.2021.107030>
75. Wang, Y., Zhang, Z., Chen, J., Fu, T.: Low-velocity impact response of agglomerated FG-CNTRC beams with general boundary conditions using Gram–Schmidt–Ritz method. *J. Braz. Soc. Mech. Sci. Eng.* **44**(11), 537 (2022). <https://doi.org/10.1007/s40430-022-03738-1>
76. Qian, L.F., Ching, H.K.: Static and dynamic analysis of 2-D functionally graded elasticity by using meshless local petrov-galerkin method. *J. Chin. Inst. Eng.* **27**(4), 491–503 (2004). <https://doi.org/10.1080/02533839.2004.9670899>
77. Abbaslou, M., Saidi, A.R., Bahaadini, R.: Vibration and dynamic instability analyses of functionally graded porous doubly curved panels with piezoelectric layers in supersonic airflow. *Acta Mech.* **234**(12), 6131–6167 (2023). <https://doi.org/10.1007/s00707-023-03699-9>
78. Ebrahimi, F., Parsi, M.: Wave propagation analysis of functionally graded graphene origami-enabled auxetic metamaterial beams resting on an elastic foundation. *Acta Mech.* **234**(12), 6169–6190 (2023). <https://doi.org/10.1007/s00707-023-03705-0>
79. Yaylacı, M., Yaylacı, E.U., Özdemir, M.E., Öztürk, Ş., Sesli, H.: Vibration and buckling analyses of FGM beam with edge crack: Finite element and multilayer perceptron methods. *Steel Compos. Struct.* (2023). <https://doi.org/10.12989/scs.2023.46.4.565>
80. Hai, T., Yvaz, A., Ali, M., Strashnov, S., El Ouni, M.H., Alkhedher, M., Eyvazian, A.X.: Effects of micromechanical models on the dynamics of functionally graded nanoplate. *Steel Compos. Struct.* **48**(2), 191 (2023). <https://doi.org/10.12989/scs.2023.48.2.191>
81. Zhang, X., Li, J., Cui, Y., Habibi, M., Ali, H.E., Albaijan, I., Mahmoudi, T.: Static analysis of 2D-FG nonlocal porous tube using gradient strain theory and based on the first and higher-order beam theory. *Steel Compos. Struct.* **49**(3), 293–306 (2023). <https://doi.org/10.12989/scs.2023.49.3.293>
82. Cho, J.R.: Neutral surface-based static and free vibration analysis of functionally graded porous plates. *Steel Compos. Struct.* **49**(4), 431 (2023). <https://doi.org/10.12989/scs.2023.49.4.431>
83. Ghatage, P.S., Sudhagar, P.E.: Free vibrational behavior of bi-directional perfect and imperfect axially graded cylindrical shell panel under thermal environment. *Struct. Eng. Mech.* **85**(1), 135–145 (2023). <https://doi.org/10.12989/sem.2023.85.1.135>
84. Tayebi, M.S., Salami, S.J., Tavakolian, M.: Free vibration analysis of FG composite plates reinforced with GPLs in thermal environment using full layerwise FEM. *Struct. Eng. Mech.* **85**(4), 445–459 (2023). <https://doi.org/10.12989/sem.2023.85.4.445>
85. Gholami, M., Azandariani, M.G., Ahmed, A.N., Abdolmaleki, H.: Proposing a dynamic stiffness method for the free vibration of bi-directional functionally-graded Timoshenko nanobeams. *Adv. Nano Res.* **14**(2), 127 (2023). <https://doi.org/10.12989/2023.14.2.127>
86. Wu, X.: Nonlinear finite element vibration analysis of functionally graded nanocomposite spherical shells reinforced with graphene platelets. *Adv. Nano Res.* **15**(2), 141–153 (2023). <https://doi.org/10.12989/anr.2023.15.2.141>
87. Xu, J.Q., She, G.L.: Thermal post-buckling and primary resonance of porous functionally graded beams: effect of elastic foundations and geometric imperfection. *Comput. Concr.* **32**(6), 543–551 (2023). <https://doi.org/10.12989/cac.2023.32.6.543>
88. Fan, J., Li, Q., Muhsen, S., Ali, H.E.: Intelligent big data analysis and computational modelling for the stability response of the NEMS. *Comput. Concr.* **31**(2), 139–149 (2023). <https://doi.org/10.12989/cac.2023.31.2.139>
89. Hadji, L., Avcar, M.: Free vibration analysis of FG Porous Sandwich Plates under various boundary conditions. *J. Appl. Comput. Mech.* **7**(2), 505–519 (2021). <https://doi.org/10.22055/JACM.2020.35328.2628>
90. Bharath, H.S., Bonthu, D., Gururaja, S., Prabhakar, P., Doddamani, M.: Flexural response of 3D printed sandwich composite. *Compos. Struct.* **263**, 113732 (2021). <https://doi.org/10.1016/j.compstruct.2021.113732>
91. Rahmani, F., Kamgar, R., Rahgozar, R.: Finite element analysis of functionally graded beams using different beam theories. *Civ. Eng. J.* **6**(11), 2086–2102 (2020). <https://doi.org/10.28991/cej-2020-03091600>

92. Katariya, P.V., Panda, S.K.: Numerical analysis of thermal post-buckling strength of laminated skew sandwich composite shell panel structure including stretching effect. *Steel Compos. Struct. Int. J.* **34**(2), 279–288 (2020). <https://doi.org/10.12989/scs.2020.34.2.279>
93. Zouatnia, N., Hadji, L.: Effect of the micromechanical models on the bending of FGM beam using a new hyperbolic shear deformation theory. *Earthq. Struct.* **16**(2), 177–183 (2019). <https://doi.org/10.12989/eas.2019.16.2.177>
94. Etemadi, E., Khatibi, A.A., Takaffoli, M.: 3D finite element simulation of sandwich panels with a functionally graded core subjected to low velocity impact. *Compos. Struct.* **89**(1), 28–34 (2009). <https://doi.org/10.1016/j.compstruct.2008.06.013>
95. Shodja, H.M., Haftbaradaran, H., Asghari, M.: A thermoelasticity solution of sandwich structures with functionally graded coating. *Compos. Sci. Technol.* **67**(6), 1073–1080 (2007). <https://doi.org/10.1016/j.compscitech.2006.06.001>
96. Arani, A.G., Zarei, H.B.A., Pourmousa, P.: Free vibration response of FG porous sandwich micro-beam with flexoelectric face-sheets resting on modified silica aerogel foundation. *Int. J. Appl. Mech.* **11**(09), 1950087 (2019). <https://doi.org/10.1142/S175882511950087X>
97. Bhangale, R.K., Ganesan, N.: Thermoelastic buckling and vibration behavior of a functionally graded sandwich beam with constrained viscoelastic core. *J. Sound Vib.* **295**(1–2), 294–316 (2006). <https://doi.org/10.1016/j.jsv.2006.01.026>
98. Anderson, T.A.: A 3-D elasticity solution for a sandwich composite with functionally graded core subjected to transverse loading by a rigid sphere. *Compos. Struct.* **60**(3), 265–274 (2003). [https://doi.org/10.1016/S0263-8223\(03\)00013-8](https://doi.org/10.1016/S0263-8223(03)00013-8)
99. Mantari, J.L., Granados, E.V.: Dynamic analysis of functionally graded plates using a novel FSDT. *Compos. B Eng.* **75**, 148–155 (2015). <https://doi.org/10.1016/j.compositesb.2015.01.028>
100. Mantari, J.L., Granados, E.V.: A refined FSDT for the static analysis of functionally graded sandwich plates. *Thin Walled Struct.* **90**, 150–158 (2015). <https://doi.org/10.1016/j.tws.2015.01.015>
101. Čukanović, D., Radaković, A., Bogdanović, G., Milanović, M., Redžović, H., Dragović, D.: New shape function for the bending analysis of functionally graded plate. *Materials* **11**(12), 2381 (2018). <https://doi.org/10.3390/ma11122381>
102. Reddy, J.N.: *Mechanics of Laminated Composite Plates: Theory and Analysis*. CRC Press, Boca Raton (1997)
103. Aydogdu, M.: Vibration analysis of cross-ply laminated beams with general boundary conditions by Ritz method. *Int. J. Mech. Sci.* **47**(11), 1740–1755 (2005). <https://doi.org/10.1016/j.ijmecsci.2005.06.010>
104. Aydogdu, M.: Buckling analysis of cross-ply laminated beams with general boundary conditions by Ritz method. *Compos. Sci. Technol.* **66**(10), 1248–1255 (2006). <https://doi.org/10.1016/j.compscitech.2005.10.029>
105. Mantari, J.L., Canales, F.G.: Free vibration and buckling of laminated beams via hybrid Ritz solution for various penalized boundary conditions. *Compos. Struct.* **152**, 306–315 (2016). <https://doi.org/10.1016/j.compstruct.2016.05.037>
106. Nguyen, T.K., Nguyen, T.T.P., Vo, T.P., Thai, H.T.: Vibration and buckling analysis of functionally graded sandwich beams by a new higher-order shear deformation theory. *Compos. B Eng.* **76**, 273–285 (2015). <https://doi.org/10.1016/j.compositesb.2015.02.032>
107. Nguyen, T.K., Vo, T.P., Nguyen, B.D., Lee, J.: An analytical solution for buckling and vibration analysis of functionally graded sandwich beams using a quasi-3D shear deformation theory. *Compos. Struct.* **156**, 238–252 (2016). <https://doi.org/10.1016/j.compstruct.2015.11.0740>
108. Tounsi, A., Tahir, S.I., Mudhaffar, I.M., Al-Osta, M.A., Chikh, A.: On the wave propagation characteristics of functionally graded porous shells. *HCMCOU J. Sci. Adv. Comput. Struct.* **14**(1), 63–80 (2024)

Publisher's Note Springer Nature remains neutral with regard to jurisdictional claims in published maps and institutional affiliations.

Springer Nature or its licensor (e.g. a society or other partner) holds exclusive rights to this article under a publishing agreement with the author(s) or other rightsholder(s); author self-archiving of the accepted manuscript version of this article is solely governed by the terms of such publishing agreement and applicable law.